ACS Catalysis

Research Article

pubs.acs.org/acscatalysis

One-Pot Synthesis of Ordered Mesoporous NiO−CaO−Al_2O_3 Composite Oxides for Catalyzing CO_2 Reforming of CH_4

Leilei Xu,[†,‡] Huanling Song,[†] and Lingjun Chou*[,†]

[†]State Key Laboratory for Oxo Synthesis and Selective Oxidation, Lanzhou Institute of Chemical Physics, Chinese Academy of Sciences, Lanzhou 730000, People's Republic of China

[‡]Graduate School of Chinese Academy of Sciences, Beijing 100049, People's Republic of China

ABSTRACT: Ordered mesoporous tricompound NiO−CaO−Al_2O_3 composite oxides with various Ca content were first designed and facilely synthesized via a one-pot, evaporation-induced, self-assembly (EISA) strategy. The obtained mesoporous materials with advantageous textural properties and superior thermal stabilities were investigated as the catalysts for the carbon dioxide reforming of methane reaction. These mesoporous catalysts entirely showed high catalytic activities as well as long catalytic stabilities toward this reaction. The improved catalytic activities were suggested to be closely associated with the advantageous structural properties, such as large specific surface areas; big pore volumes; and uniform pore sizes, which could provide sufficient "accessible" active centers for the gaseous reactants. In addition, the "confinement effect" of the mesoporous matrixes contributed to stabilizing the Ni active sites during the processes of reduction and reaction, accounting for the long lifetime stabilities of these mesoporous catalysts. The modification of Ca played dual roles in promoting the catalytic activities and suppressing the carbon deposition by enhancing the chemisorption of the CO_2. Generally, the ordered mesoporous NiO−CaO−Al_2O_3 composite oxides could be considered as promising catalysts for the carbon dioxide reforming of methane reaction.

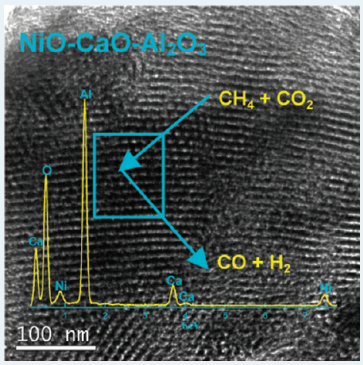

KEYWORDS: *one-pot synthesis, ordered mesopores, confinement effect, NiO−CaO−Al_2O_3, carbon dioxide reforming, methane*

1. INTRODUCTION

There has been great interest in recent years in highly efficient utilization of natural gas (mainly methane) and in the reduction of carbon dioxide in the atmosphere in view of environmental protection as well as potential industrial applications.[1−6] Herein, the catalytic process of CO_2 reforming of methane (CRM) provides one of the attractive and promising routes for the effective use of CH_4 and CO_2 resources, which consumes two greenhouse gases simultaneously to produce valuable synthesis gas.[1,2,6] The product mixture of this reaction has a relatively lower H_2/CO ratio (1/1) than those of steam reforming (3/1) and partial oxidation (2/1) of methane, which is more desirable for direct use as feedstock for oxo synthesis, synthesis of oxygenates, etc.[7−9] Furthermore, considering its strong endothermic feature, this reforming process can also be applied in chemical energy transmission systems to convert inexpensive nuclear and solar energies into valuable chemical energy.[10,11] However, so far, no industrial practice has been established for this catalytic reaction system, mainly due to the absence of an effective and economic catalyst. Therefore, developing efficient and economical catalysts remains a challenging task encountered in current research.[2,12]

During the past decades, numerous catalyst systems have been extensively investigated with the aim to understand the reaction mechanism and to optimize the process parameters.[2,12−14] Both supported noble metals, such as Rh, Ru, Pt, Pd, Ir, etc,[1,15−20] and Ni -based catalysts have showed good catalytic activities toward the CRM reaction;[21,22] however, the fatal drawback of the Ni-based catalysts is the rapid deactivation deriving from carbon deposition and the thermal sintering of the active centers.[2,12,23] Although noble metal catalysts performed good resistance toward carbon deposition, they were not economical enough for large-scale applications, considering their high cost and limited availability. Consequently, it is more practical to explore stable and active Ni-based catalysts.

Pioneer studies have indicated that the size of the Ni particles has a crucial role in suppressing coke.[2,3,13,24−26] It has been reported that carbon deposition can occur only when the metal cluster is greater than a critical size. Therefore, to inhibit carbon deposition, one must ensure that the size of the metal cluster is smaller than the critical size needed for coke formation.[24,27] However, controlling the size of Ni nanoparticles is not so straightforward because the thermal sintering of the nanosized Ni particles easily takes place under severe reduction and reaction conditions, especially for supported catalysts, due to its low Tammann temperature.[28,29]

In view of the disadvantages of conventional supported catalysts, the materials with "well-defined" structures, such as perovskites,[30,31] hexaaluminates,[32,33] spinels,[34] solid solutions,[3,21,24,34,35] and so on, can be considered as promising sources of small metal particles. Nanosized Ni particles can be

Received: February 12, 2012
Revised: April 27, 2012
Published: May 22, 2012

obtained in situ under a reduction environment. The thermal sintering of Ni nanoparticles is efficiently suppressed as a result of the confinement role of these "well-defined" structures. Nevertheless, compared with porous catalysts, the structural properties, such as specific areas, pore volumes, pore size distributions, and so on, of these "well-defined" structure materials are not excellent enough to meet the demand of this reaction. In other words, they are not able to provide sufficient "accessible" active centers for the reactants.

Furthermore, the catalysts with Lewis basic sites generally results in enhancing the catalytic activity and lowering the coke deposition rate.[36,37] The presence of Lewis basic centers in catalysts could promote chemisorption of the CO_2 during the CRM reaction and accelerate the process of eliminating coke through the course that CO_2 reacts with the deposited coke to form CO (specifically, $CO_2 + C = 2CO$), finally improving the stability of the catalyst. Therefore, alkali metal oxides (such as Na_2O, K_2O, Cs_2O), alkaline earth metal oxides (such as MgO, CaO, BaO), and some rare earth oxides (such as La_2O_3, Sm_2O_3) are usually selected as basic supports or modifiers.[37−42]

On the basis of the principle mentioned above, a group of tricompound NiO−CaO−Al_2O_3 materials with ordered mesoporous structures was originally designed and facilely synthesized via a one-pot, evaporation-induced, self-assembly (EISA) strategy. The received mesoporous materials possessing predominant textural properties and thermal stabilities were investigated as catalysts for the CRM reaction. To the best of our knowledge, there has been almost no literature reporting the facile synthesis of the tricompound ordered mesoporous NiO−CaO−Al_2O_3 composite oxide materials and employing them as catalysts for the CRM reaction. More details about the synthesis of these mesoporous materials and their catalytic properties for CRM reaction are described specifically in the following text.

2. EXPERIMENTAL SECTION

2.1. Synthesis of Ordered Mesoporous NiO−CaO−Al_2O_3 Composite Oxides. Aluminum isopropoxide ($C_9H_{21}AlO_3$, 98+%, Sigma-Aldrich), $(EO)_{20}(PO)_{70}(EO)_{20}$ triblock copolymer (Pluronic P123, typical M_n = 5800, Sigma-Aldrich), 67 wt % nitric acid (HNO_3, Baiyin Liangyou Chemical Reagent Co. Ltd.), nickel nitrate hexahydrate ($Ni(NO_3)_2{\cdot}6H_2O$, Shanghai NO.2 Reagent Factory, China), calcium nitrate tetrahydrate ($Ca(NO_3)_2{\cdot}4H_2O$, Beijing Shuanghuan Reagent Factory, China), and absolute ethanol (C_2H_5OH, Sinopharm Chemical Reagent Co. Ltd.) employed in this study were all A.R. grade. All the chemicals were used as received without further purification.

Since a reliable and reproducible preparation method for the synthesis of the ordered mesoporous alumina (OMA) was reported by Yuan et al.,[43] this method had been improved by Morris et al. to synthesize OMA-supported metal oxide binary systems.[44] Their work inspired us to further extend this strategy to a one-pot synthesis NiO−CaO−Al_2O_3 ternary system. Currently, ordered mesoporous x mol % NiO/y mol % CaO/z mol % $AlO_{3/2}$ (x mol % = $n_{Ni}/(n_{Ni} + n_{Ca} + n_{Al}) \times 100\%$, $x + y + z = 100$, denoted as M-xNiyCazAl in the following text) composite metal oxides were successfully synthesized via improved one-pot, evaporation-induced, self-assembly (EISA) by fine control of the volatilization process.

In a typical synthesis procedure, ∼1.0 g $(EO)_{20}(PO)_{70}(EO)_{20}$ of triblock copolymer was dissolved in 20.0 mL of anhydrous ethanol with vigorous stirring. Then 1.6 mL of 67 wt % nitric acid, approximately A mmol aluminum isopropoxide, B mmol nickel nitrate hexahydrate, and C mmol calcium nitrate tetrahydrate ($A + B + C = 10$ mmol) were added into the above solution in sequence with vigorous stirring. The final mixture was covered with PE film and stirred at room temperature for at least 5 h. Finally, the mixture was transferred to a Petri dish, the Petri dish was covered with PE film with holes, and the covered Petri dish was placed into a 60 °C drying oven to undergo the slow EISA process for 48 h. A light green solid xerogel was obtained after 48 h via precise control of the EISA process. The final gel was calcined by slowly increasing the temperature (1 °C/min ramping rate) to 600 °C and keeping it at the final temperature for 5 h. As a result, the M-xNiyCazAl composite metal oxide powders with large BET specific surface areas, big pore volumes, and narrow pore size distributions were obtained. The as-prepared mesoporous materials were pressed; crushed; sieved through 20−40 meshes; and finally, reserved as catalysts for the CRM reaction.

2.2. Characterization. Powder X-ray diffraction (XRD) measurements were performed using an X'Pert Pro multipurpose diffractometer (PANalytical, Inc.) with Ni-filtered Cu Kα radiation (0.150 46 nm) at room temperature from 0.6° to 5.0° (small angle) and from 10.0° to 80.0° (wide angle). Measurements were conducted using a voltage of 40 kV, current setting of 40 mA, step size of 0.02°, and count time of 4 s. The nitrogen adsorption and desorption isotherms at −196 °C were recorded on an Autosorb-iQ analyzer (Quantachrome Instruments, Boynton Beach, FL). Prior to the tests, samples were degassed at 200 °C for 4 h. The specific surface areas were calculated via the BET method in the relative pressure range of 0.05−0.3; the single-point pore volume was calculated from the adsorption isotherm at a relative pressure of 0.990; pore size distributions were calculated using adsorption branches of nitrogen adsorption−desorption isotherms by the BJH method. Transmission electron microscopy (TEM) images, selected area electron diffraction (SAED) and energy-dispersive X-ray spectroscopy (EDX) measurements were performed on a JEM-2010 (Japan) high-resolution transmission electron microscopy under a working voltage of 200 kV. X-ray photoelectron spectroscopy (XPS) analyses of the catalysts were performed on a Thermo Fisher Scientific K-Alpha spectrometer.

Prior to the test, the fresh catalyst was placed on a sample holder and pressed into a self-supported wafer. Thermogravimetric−differential scanning calorimetry (TG−DSC) measurements were carried out on a NETZSCH STA 449F3 thermogravimetric analyzer from room temperature to 900 °C at a rate of 10 °C/min under air atmosphere. H_2 temperature programmed reduction (H_2-TPR) measurements were performed on an AMI-100 unit (Zeton-Altamira instrument, Pittsburgh, PA) employing hydrogen as the reducing agent. The samples (250 mg) were loaded in a U-shaped quartz reactor. Prior to the TPR measurements, samples were pretreated at 300 °C for 0.5 h in flowing He (50 mL/min) to remove any moisture and adsorbed impurities. After cooling the reactor to room temperature, a 5 mol % H_2−He (50 mL/min) gas mixture was introduced. The catalyst was heated to 1000 °C at a rate of 10 °C/min, and the hydrogen consumption was measured using an AMETEK (LC-D-200 Dycor AMETEK) mass spectrometer. CO_2 temperature-programmed desorption (CO_2-TPD) measurements were carried out on the same apparatus as described for H_2-TPR. The sample (150 mg) was pretreated at 300 °C for 2 h in a He stream (50 mL/min). After being cooled to 20 °C, the

dx.doi.org/10.1021/cs3001072 | ACS Catal. 2012, 2, 1331−1342

pretreated sample was exposed in pure CO_2 atmosphere for 30 min, then the sample was purged with a He airstream until the baseline of CO_2 in the mass spectrum was steady. Finally, the CO_2-TPD was carried out with a ramp of 20 °C/min from 20 °C to the needed temperature under He stream.

2.3. Catalytic Activity Measurements. Catalytic tests were performed at atmospheric pressure in a vertical fixed-bed, continuous flow, quartz reactor (8 mm i.d.). The whole reaction evaluation system consisted of a mass flow controller unit (MT50-4J Metron Instruments), a reactor unit, and an analysis unit (SP-6800A GC). The reaction temperature increased from 600 to 800 °C in 50 °C increments. The analysis for the effluent gas was carried out after stabilizing for 1 h at each studied temperature and gas hourly space velocity (GHSV). Typically, 100 mg of catalyst diluted with 350 mg of quartz sand (20−40 meshes) was used in each run. Prior to the reaction, the catalyst was reduced in situ in a mixed flow of H_2 and N_2 (H_2/ N_2 = 10:20 mL/min) with a heating rate of 1.5 °C/min to 800 °C and maintained at 800 °C for 120 min. Before introducing the reaction gases, the catalyst bed was purged with N_2 for half an hour to remove the absorbed hydrogen, then the reaction mixture was fed into the reactor via the flow controller unit. The effluent gases were cooled in an ice−water trap to remove the gaseous water generating by a reverse water−gas shift (RWGS) reaction. The separation and quantification of the products were achieved on an online chromatograph equipped with a TDX-01 packed column.

3. RESULTS AND DISCUSSION

3.1. Characterization of As-Prepared M-5Ni*x*Ca(95 − *x*)Al Materials. *3.1.1. XRD Analysis.* The small-angle X-ray diffraction (SXRD) had been widely used in the study of the ordered mesoporous material, such as MCM-41, to assess the two-dimensional structure of the sample.[45,46] The SXRD patterns of the as-prepared M-5Ni*x*Ca(95 − *x*)Al materials calcined at 600 °C were displayed in Figure 1 (1). Most of the samples showed a strong diffraction peak around 0.7−0.9° and one weak peak around 1.4−1.6°, which, combined with the TEM observations could be indexed as (1 0 0) and (1 1 0) reflections of *p6mm* two-dimensional hexagonal structure, respectively. Therefore, ordered mesoporous NiO−CaO−Al_2O_3 with various Ca molar contents were facilely prepared and the ordered mesoporous frameworks were successfully preserved after being calcined at 600 °C, demonstrating good thermal stability. Figure 1 (2) presents the wide-angle X-ray diffraction (WXRD) patterns of the above-mentioned materials. The WXRD patterns for all the materials behaved no apparent NiO, CaO and even Al_2O_3 diffraction peaks, illustrating the high dispersion of the NiO and CaO among the amorphous mesoporous skeleton of the materials. In the M-5Ni*x*Ca(95 − *x*)Al materials, Ni and Ca atoms were supposed to be inlaid in the mesoporous frameworks and segregated by the Al_2O_3 substrate as a result of the special advantages of the one-pot preparation strategy; therefore, the thermal agglomeration of the NiO nanoparticles during the process of the calcination was avoided to some extent, accounting for the high dispersion of NiO particles.

3.1.2. Nitrogen Adsorption−desorption Analysis. Similar to the XRD characterization, nitrogen physisorption could also provide the bulk information of the porous materials. The nitrogen adsorption and desorption isotherms as well as their pore size distributions are displayed in Figure 2. As shown in Figure 2(1), for all the as-prepared M-5Ni*x*Ca(95 − *x*)Al

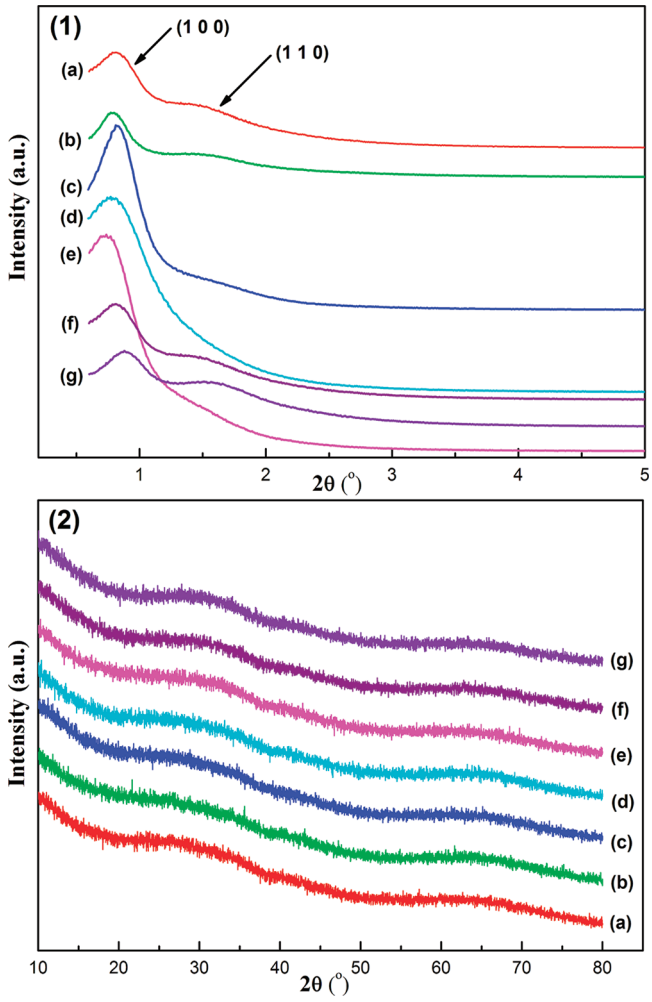

Figure 1. Small-angle X-ray diffraction (1) and wide-angle X-ray diffraction (2) patterns of the M-5Ni*x*Ca(95 − *x*)Al materials calcined at 600 °C: (a) M-5Ni95Al, (b) M-5Ni1Ca94Al, (c) M-5Ni2Ca93Al, (d) M-5Ni3Ca92Al, (e) M-5Ni5Ca90Al, (f) M-5Ni8Ca87Al, and (g) M-5Ni10Ca85Al.

materials calcined at 600 °C, their isotherms were attributable to IV type isotherms with H1 shaped hysteresis loops, which were the significant features for the ordered mesoporous materials. Furthermore, nearly all the capillary condensation steps of the hysteresis loops were very steep, suggesting the presence of the mesopores with excellent uniformity among the framework of M-5Ni*x*Ca(95 − *x*)Al materials. The H1-shaped hysteresis loops also illuminated that all the mesopores were "cylindrically shaped" channels, which would be confirmed by the TEM images. In addition, the pore size distributions of these materials exhibited in Figure 2(2) were all extremely narrow, and the positions of the peaks of the curves were located in the range of 6.5−12.0 nm, belonging to "mesopore" on the basis of the definition of IUPAC (2.0−50.0 nm).

In addition, the textural properties of the as-prepared M-5Ni*x*Ca(95 − *x*)Al materials with varieties of Ca contents were summarized in Table 1. It could be observed that all the samples possessed large specific surface areas up to 222 m^2/g and big pore volumes up to 0.48 cm^3/g. Without exception, the average pore diameters of the materials were located in the range of 6.5−12.0 nm, whereas, it is worth noting that incorporating the Ca element into the mesostructure seemingly resulted in some decrease in specific surface areas and pore

dx.doi.org/10.1021/cs3001072 | ACS Catal. 2012, 2, 1331−1342

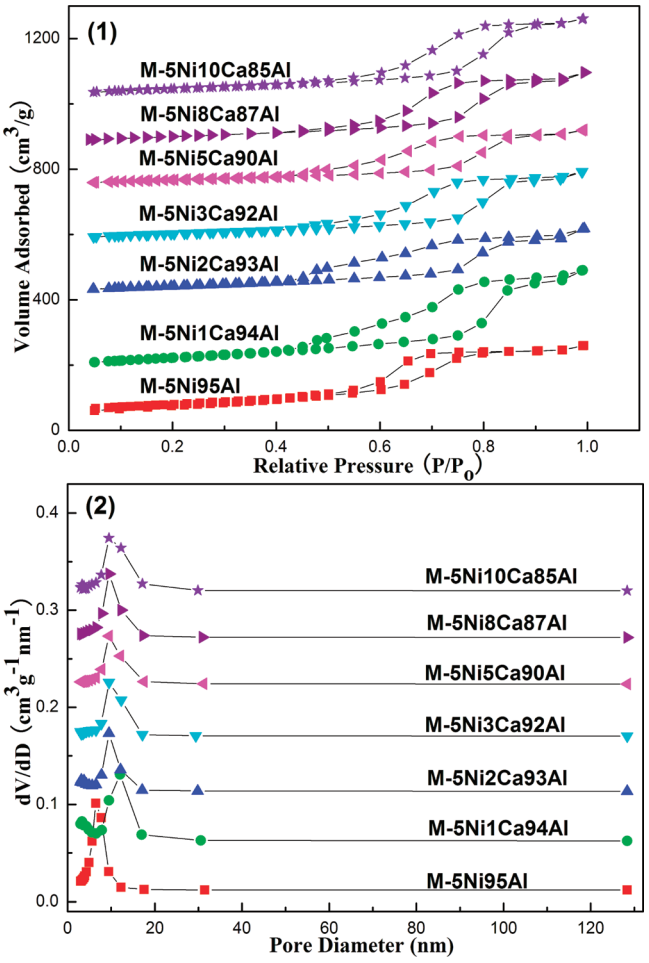

Figure 2. Isotherms (1) and pore size distributions (2) of the M-5Ni*x*Ca(95 − *x*)Al materials calcined at 600 °C.

volumes to some extent. This phenomenon had been encountered in the pioneer literature reporting ordered mesoporous alumina-supported metal oxides.[44,47]

3.1.3. TEM Analysis. M-5Ni5Ca90Al, M-5Ni8Ca87Al, and M-5Ni10Ca85Al were selected as representatives of ordered M-5Ni*x*Ca(95 − *x*)Al materials with various Ca contents. Their TEM images are expressly displayed in Figure 3a−f. The highly ordered hexagonal arrangement of the pores along the [001] direction (Figure 3b, d, f) and the alignment of cylindrical pores along the [110] (Figure 3a, c, e) direction were distinctly observed for all the selected representatives. These TEM images were in good agreement with the characterization results of the SXRD, which predicted the presence of ordered mesopores with *p6mm* two-dimensional hexagonal symmetry. The cylindrical pores along [110] further confirmed the deduction based on the H1-shaped hysteresis loops in nitrogen adsorption and desorption analysis.

As for the M-5Ni95Al not being modified by Ca, its TEM images related to ordered mesopores were reflected in our previous work.[48] The SAED patterns of the mesostructure domains were also provided in the inlets of Figure 3a, c, e; however, there was no apparent diffuse electron diffraction rings observed in SAED patterns, indicating that the crystallinity of the mesoporous frameworks was not very good. The results of the SAED were consistent with those of the WXRD. In addition, the EDX measurement of the ordered mesostructure domains for M-5Ni10Ca85Al was also conducted, and its profile is shown in Figure 2g. The exclusive peaks for Ni, Ca, Al, and O were clearly observed, implying that all the metallic elements were successfully introduced into ordered mesoporous frameworks.

Table 1. Textural Properties of the As-Prepared M-5Ni*x*Ca(95 − *x*)Al Materials Calcined at 600 °C, As-Reduced M-5Ni5Ca90Al, the Used M-5Ni5Ca90Al, and the Endurance-Tested M-5Ni5Ca90Al Catalysts

samples	specific surface area (m^2/g)	pore volume (cm^3/g)	average pore diameter (nm)	isotherm type
M-5Ni95Al	222	0.44	6.75	IV H1
M-5Ni1Ca94Al	201	0.48	12.05	IV H1
M-5Ni2Ca93Al	128	0.32	9.50	IV H1
M-5Ni3Ca92Al	132	0.35	9.49	IV H1
M-5Ni5Ca90Al	110	0.28	9.48	IV H1
M-5Ni8Ca87Al	127	0.36	9.57	IV H1
M-5Ni10Ca85Al	143	0.39	9.51	IV H1
the as-reduced M-5Ni5Ca90Al[a]	59	0.17	9.47	IV H1
the used M-5Ni5Ca90Al[b]	56	0.16	9.68	IV H1
the endurance test M-5Ni5Ca90Al[c]	61	0.18	9.58	IV H1

[a]The M-5Ni5Ca90Al catalyst was in situ reduced under H_2/N_2 (H_2/N_2 = 10:20 mL/min) atmosphere at 800 °C for 2 h. [b]The used catalyst was the catalyst tested under the following conditions: CH_4/CO_2 = 1, GHSV = 15000 mL/(g·h), 1 atm, and temperature from 600 to 800 °C with an increment of 50 °C, and remaining at each temperature stage for 70 min. [c]The M-5Ni5Ca90Al material was used as the catalyst of the carbon dioxide reforming of methane reaction for a 50 h long-term stability test. Reaction conditions: CH_4/CO_2 = 1, GHSV = 15000 mL/(g·h), 700 °C, 1 atm.

3.1.3. XPS Analysis. Being sensitive to the composition of the top surface layers, XPS measurement was commonly used to determine the state of the surface element species in the materials. Table 2 provides the binding energies of the surface elements of the M-5Ni*x*Ca(95 − *x*)Al materials with different Ca contents. It was found that the binding energies of the surface elements Ni, Al, and O were not affected by Ca's modification with various contents; that is, their valence states were basicallyunchanged. Therefore, the addition of the Ca did not alter the electronic environment of these ions on the basis of the uniformity of their binding energies. On the basis of the standard binding energy data, it could be concluded that their oxidation states were Ni^{2+}, Ca^{2+}, Al^{3+}, and O^{2-}, respectively. In addition, the XPS profiles of Ni2p for these as-prepared materials are exhibited in Figure 4. It was observed that the position of the $Ni_{2p3/2}$ peak was centered around 856.0 eV and accompanied by an uptake satellite peak at 862.0 eV for each sample, which was the typical characteristic of nickel species for $NiAl_2O_4$ spinel, according to the pioneer literature.[32,49−51] However, as a matter of fact, the binding energy of the $Ni_{2p3/2}$ in pure NiO was ~853.30 eV. Therefore, the Ni species in M-5Ni*x*Ca(95 − *x*)Al might present itself in the form of $NiAl_2O_4$ spinel-like species instead of free or dissociated NiO. The following H_2-TPR measurement would further confirm this assumption.

3.1.4. H_2-TPR analysis. The TPR technique was an effective means for determining the reducibility of the metal oxide based supported catalysts, which further provided information about the interactions between metal oxides and their supports. H_2-TPR profiles of the as-synthesized M-5Ni*x*Ca(95 − *x*)Al

dx.doi.org/10.1021/cs3001072 | ACS Catal. 2012, 2, 1331−1342

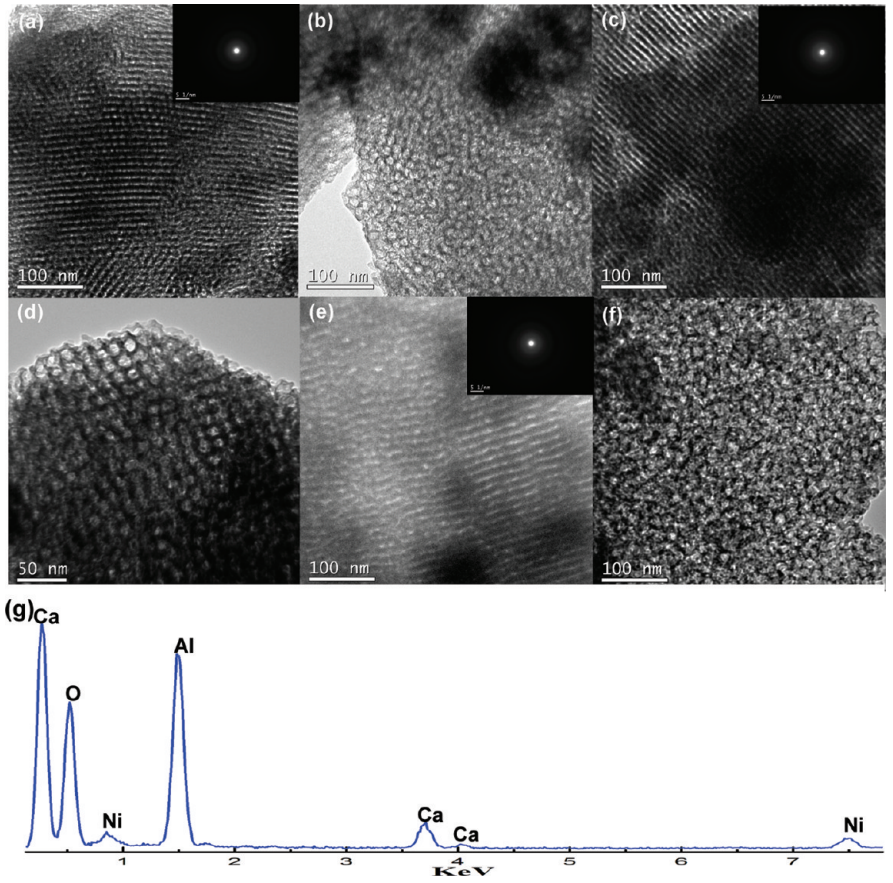

Figure 3. TEM images of as-synthesized M-5Ni*x*Ca(95 − *x*)Al materials calcined at 600 °C: (a, b) M-5Ni5Ca90Al, (c, d) M-5Ni8Ca87Al, (e, f) M-5Ni10Ca85Al. (g) EDX measurement for M-5Ni10Ca85Al.

Table 2. Binding Energies (eV) of the Surface Elements of the As-Prepared M-5Ni*x*Ca(95 − *x*)Al Materials

x	Ca2p	$Ni2p_{3/2}$	Al2p	,O1s
0		856.22	74.31	531.47
1	347.65	856.24	74.44	531.43
2	347.56	856.42	74.45	531.53
3	347.43	856.28	74.35	531.44
5	347.39	856.19	74.32	531.41
8	347.35	856.25	74.27	531.47
10	347.35	856.25	74.27	531.47

samples are shown in Figure 5. All the samples exhibited similar profiles of hydrogen reduction, showing only one obvious reduction peak for each sample in the region from 735 to 790 °C, regardless of the Ca content. No evident reduction peak in the range of 300−400 °C was observed, implying the absence of a dissociated or free NiO.[52−54] This evidence apparently confirmed that the strong interactions between the Ni and the ordered mesoporous framework, such as $NiAl_2O_4$ spinel-like species based on the above XPS analysis, had been established.

In addition, it was worth noting that, compared with M-5Ni95Al, the reduction peak gradually migrated toward relatively lower temperatures with the increase in the Ca content for most of the materials studied, which had been encountered in the previous works.[40,55] The reason for this trend might derive from the competition between Ni and Ca for interacting with the alumina substrate. Ca would tend to form calcium aluminate ($CaAl_2O_4$), reducing the opportunity of the subsequent formation of the nickel aluminate

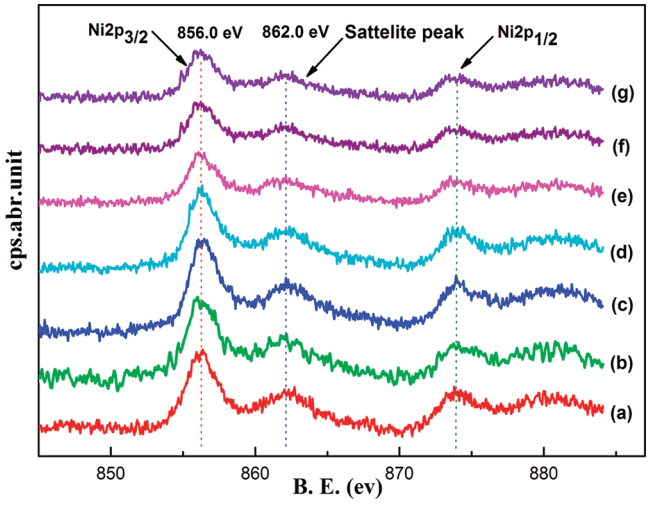

Figure 4. XPS spectra of the Ni2p in M-5Ni*x*Ca(95 − *x*)Al materials calcined at 600 °C with different Ca contents: (a) M-5Ni95Al, (b) M-5Ni1Ca94Al, (c) M-5Ni2Ca93Al, (d) M-5Ni3Ca92Al, (e) M-5Ni5Ca90Al, (f) M-5Ni8Ca87Al, and (g) M-5Ni10Ca85Al.

($NiAl_2O_4$).[40,55] The sample with higher Ca content might present a weaker interaction toward alumina, finally resulting in the reduction of the Ni species at lower temperatures. Generally, the high reduction temperatures of the Ni species H_2-TPR analysis were in good agreement with the conclusion: the presence of $NiAl_2O_4$ spinel-like species based on the XPS characterization.

dx.doi.org/10.1021/cs3001072 | *ACS Catal.* 2012, 2, 1331−1342

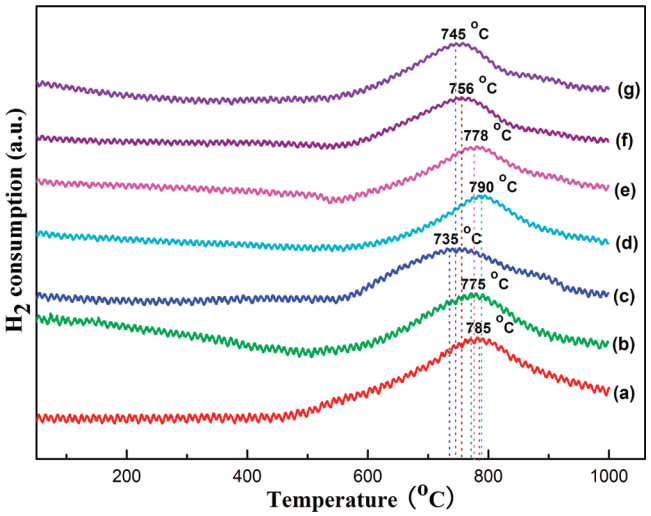

Figure 5. H_2-TPR profiles of the M-5Ni*x*Ca(95 − *x*)Al materials calcined at 600 °C with different Ca content: (a) M-5Ni95Al, (b) M-5Ni1Ca94Al, (c) M-5Ni2Ca93Al, (d) M-5Ni3Ca92Al, (e) M-5Ni5Ca90Al, (f) M-5Ni8Ca87Al, and (g) M-5Ni10Ca85Al.

3.1.5. CO_2-TPD Analysis. CO_2-TPD analysis was carried out to determine the surface basicity of the materials. Commonly, it was believed that CO_2 adsorbed on weaker basic sites would be desorbed at lower temperatures, and that adsorbed on stronger basic sites would be desorbed at higher temperatures.[56] The CO_2-TPD profiles of the as-synthesized M-5Ni*x*Ca(95 − *x*)Al samples with various Ca content are compared in detail in Figure 6. Generally, the TPD profiles for all the samples were

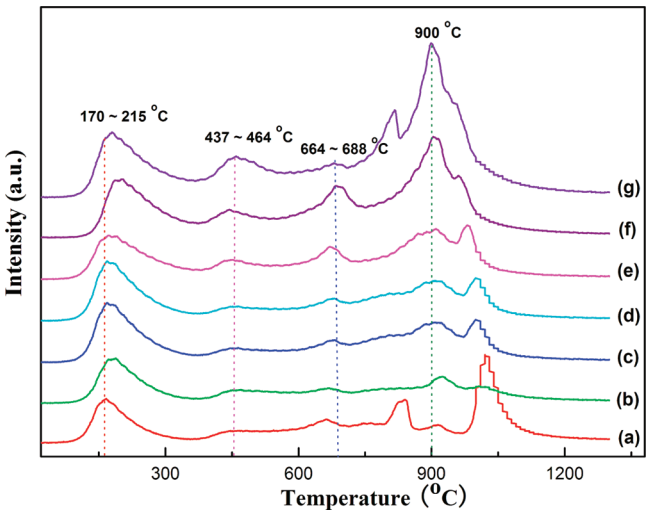

Figure 6. CO_2-TPD profiles of the M-5Ni*x*Ca(95 − *x*)Al materials calcined at 600 °C with different Ca contents: (a) M-5Ni95Al, (b) M-5Ni1Ca94Al, (c) M-5Ni2Ca93Al, (d) M-5Ni3Ca92Al, (e) M-5Ni5Ca90Al, (f) M-5Ni8Ca87Al, and (g) M-5Ni10Ca85Al.

very similar in shape. It could be clearly seen that all the materials presented a strong and broad CO_2 desorption peak in the region of 170−215 °C. Especially, it could also be observed that the M-5Ni95Al without any Ca modification still possessed an intense desorption peak around 170 °C. Furthermore, it was also of great interest to find that, with an increase in the Ca content, the intensities of these desorption peaks increased and the vertices of the desorption peaks experienced a little migration toward higher temperatures from 170 to 215 °C. Therefore, on the basis of the aforementioned phenomena, it could speculated that the desorption peak around 170 °C might be not only derived from the weakly chemisorbed CO_2 but also physically adsorbed CO_2 due to the large pore volumes and specific surface areas.

As for the desorption peaks located in the range of 437−464 °C, they might be related to the basic sites with moderate intensities. The amount of Ca markedly affected the intensities of these peaks. However, the relationship between the intensities of desorption peaks ranged from 664 to 688 °C, and the Ca content seemed a bit confusing. Specifically, the M-5Ni10Ca85Al with the highest Ca content exhibited the lowest CO_2 desorption intensity. The desorption peaks around 900 °C might be caused by the thermal decomposition of the $CaCO_3$ ($CaCO_3 \rightarrow CO_2 + CaO$), which could initially decompose at 825 °C. Their intensities were also closely related to the Ca content. In general, it was certain that the M-5Ni*x*Ca(95 − *x*)Al materials with different categories of basic centers would definitely affect their catalytic properties, such as catalytic activities, coke resistant properties, etc., which is comprehensively discussed in the following text.

3.2. Catalytic Performances of the CRM Reaction over M-5Ni*x*Ca(95 − *x*)Al Catalysts. *3.2.1. Effect of Reaction Temperature.* A blank test was performed prior to the regular catalytic experiments and showed almost no catalytic activity, even at temperatures as high as 800 °C. The catalytic performances of the M-5Ni*x*Ca(95 − *x*)Al with various Ca molar percentages in CRM reaction at different temperatures under the given reaction conditions (GHSV = 15 000 mL/(g·h), CH_4/CO_2 = 1, 1 atm) are shown in Figure 7. As shown in Figure 7(1) and (2), the conversions of CH_4 and CO_2 were largely dependent on the reaction temperatures. Especially, with the increase of the reaction temperatures, the conversions of the CH_4 and CO_2 were significantly elevated, revealing the intensely endothermic feature of the CRM reaction. Therefore, all the catalysts performed their highest catalytic activities at 800 °C in the temperature range studied.[2]

In addition, as shown in Figure 7(3), the H_2/CO ratio was also closely related to the reaction temperature. Generally, the H_2/CO ratios for all the temperatures investigated were always lower than the stoichiometric ratio (1/1) of the CRM reaction. The reason for this was that the CRM reaction was usually accompanied by the RWGS reaction ($CO_2 + H_2 = CO + H_2$), in which H_2, one of the two main products of the CRM reaction, was partly consumed, finally leading to the relatively lower ratio than that of the stoichiometric ratio. Furthermore, it could also be observed that the H_2/CO ratios increased as the reaction temperature increased. The reason for this phenomenon might also derive from the RWGS reaction, which could be gradually suppressed with an increase in the reaction temperature, on the basis of the thermodynamic analysis.

In addition to this, the relationship between the catalytic activity and the molar fraction of the Ca modifiers also could be observed in Figure 7(1) and (2). It was of great interest to find that all the M-5Ni*x*Ca(95 − *x*)Al catalysts displayed similar catalytic activities, regardless of the Ca content, implying that they could provide sufficient Ni active sites for the gaseous reactants under this given condition.

In addition, it is worth noting that CH_4, CO_2 conversions of these mesoporous catalysts had been close to or even exceeding their respective thermodynamic equilibrium conversion in the temperature ranges studied. The superior catalytic properties

dx.doi.org/10.1021/cs3001072 | ACS Catal. 2012, 2, 1331−1342

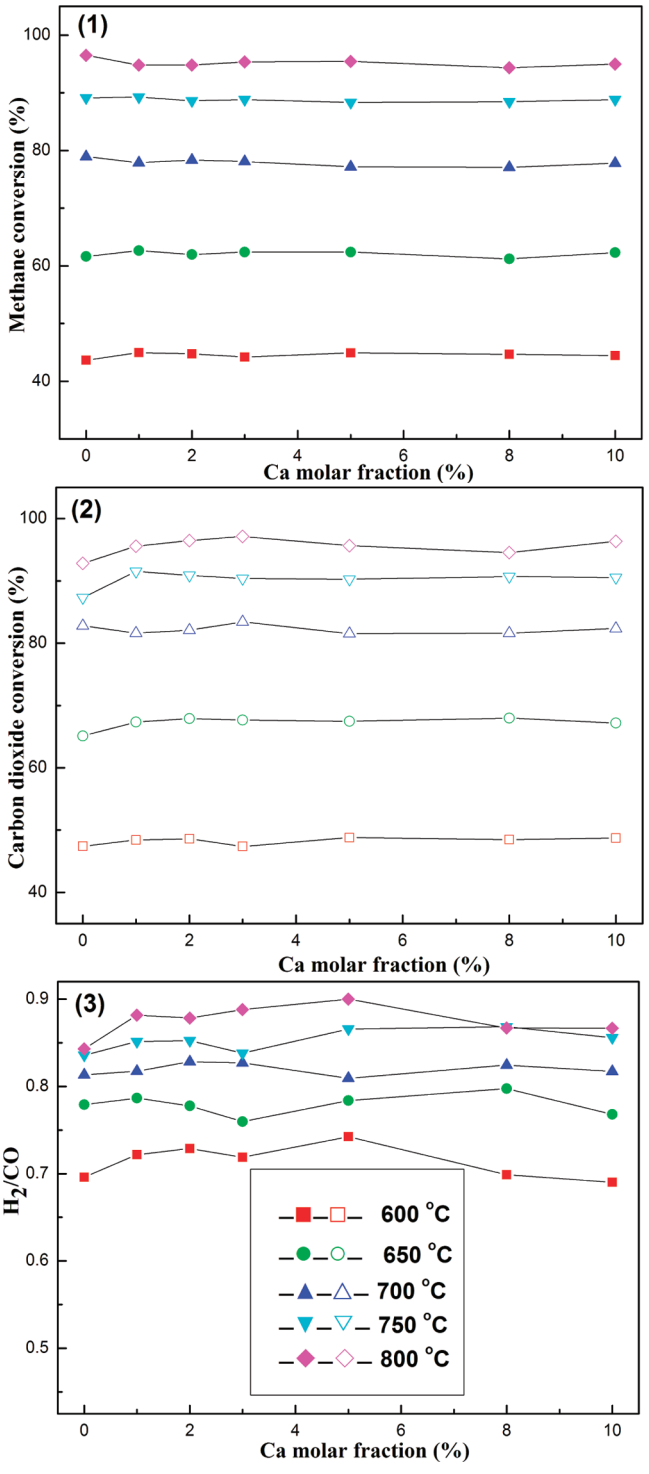

Figure 7. The curves of the (1) CH_4 conversions, (2) CO_2 conversions, (3) H_2/CO ratios versus Ca molar fraction at different reaction temperatures., Reaction conditions: CH_4/CO_2 = 1, GHSV = 15000 mL/(g·h), 1 atm.

for these mesoporous catalysts might derive from the textural properties, such as large specific surface areas and pore volumes, of these mesoporous catalysts, which could provide more "accessible" Ni active centers for the gaseous reactants, finally leading to better catalytic activity. In addition, the relationships between the H_2/CO ratios and the Ca loading also could be observed in Figure 7(3); however, their connections were, indeed, complicated, and no rule was to follow.

3.2.2. Effect of Gas Hourly Space Velocity (GHSV). As shown in Figure 8, the impact of the GHSV on the CH_4, CO_2 conversions as well as the H_2/CO ratios was also carefully studied under specific conditions (CH_4/CO_2 = 1, 750 °C, 1 atm) over M-5Ni*x*Ca(95 − *x*)Al catalysts. It was found in Figure 8(1) and (2) that the CH_4, CO_2 conversions suffered rapid decrease (e.g., from 89.11% to 67.27% for the CH_4 conversion over M-5Ni95Al) with an increase in the feed flow

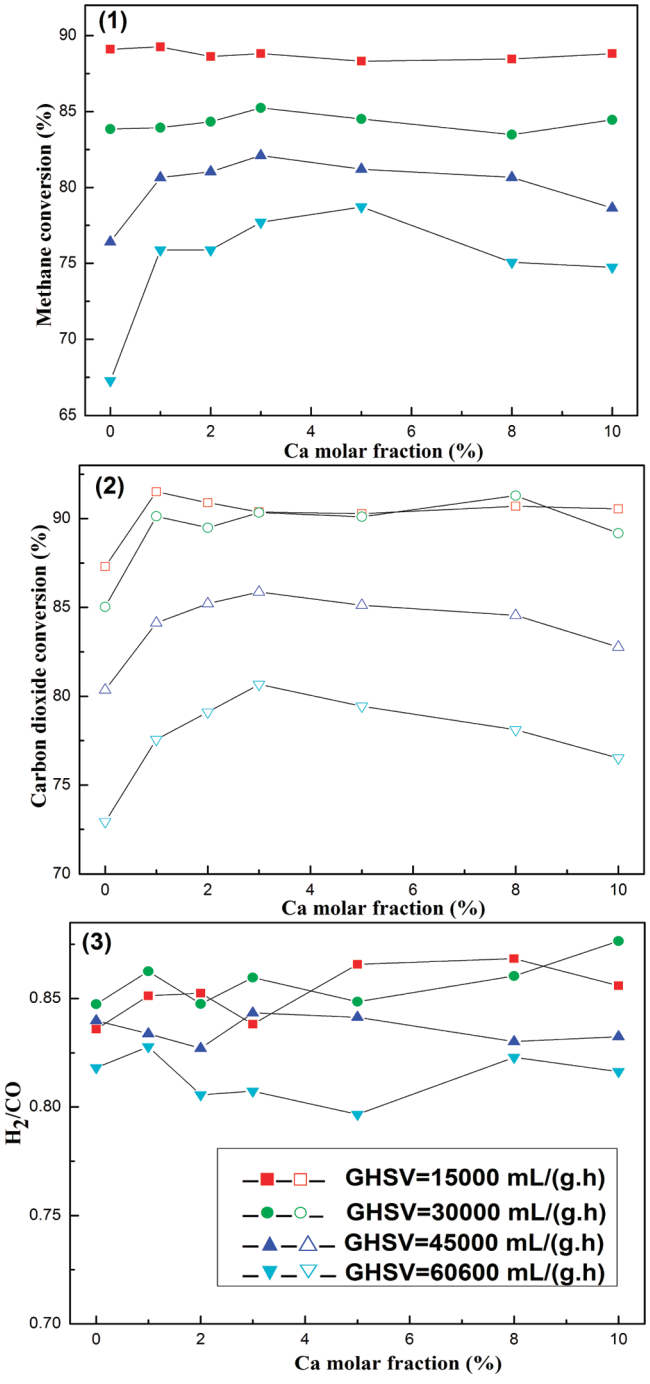

Figure 8. The curves of the (1) CH_4 conversions, (2) CO_2 conversions, (3) H_2/CO ratios versus Ca molar fraction at various gas hourly space velocities (GHSV). Reaction conditions: CH_4/CO_2 = 1, 750 °C, 1 atm.

dx.doi.org/10.1021/cs3001072 | *ACS Catal.* 2012, 2, 1331−1342

rate from 15 000 to 60 600 mL/(g·h). On the basis of the previous literature, it was believed that it was the decrease in the residence time on the surface of the catalyst and limited active centers for the increasing number of the reactants that caused the decline in the catalytic conversions.[22,40] In addition, it also could be observed in Figure 8(3) that the general trend of the H_2/CO ratios suffered some decline as the GHSV increased for most of the catalysts. Similar to Figure 7(1) and (2), the influence of the Ca basic modifier on the catalytic activities over M-5NixCa(95 − x)Al catalysts was also expressly reflected in Figure 8(1) and (2). As mentioned in the above section, all the catalysts behaved in a manner similar to CH_4 and CO_2 conversions, regardless of the Ca molar ratio, when the GHSV was kept at 15 000 mL/(g·h).

As the GHSV increased from 15 000 to 60 600 mL/(g·h), the CH_4, CO_2 conversions of mesoporous catalysts modified by Ca were higher than those of the M-5Ni95Al, and their advantages became more and more remarkable. However, the role of the Ca for the catalysts with modifiers became complicated to some degree. Typically, when the Ca content initially increased from 1% to 3%, the CH_4 and CO_2 conversions, particularly for higher GHSV, presented some increase. In contrast, an excessive amount of Ca acted in an opposite manner. With the further addition of Ca up to 10%, the catalytic activities suffered a certain degree of decrease. It is necessary to explain these unique phenomena caused by the addition of Ca. Generally, these curves, especially those at higher GHSV (45 000, 60 600 mL/(g·h)), were similar to the "volcano-shaped curve" in the shape, which was fairly popular in the field of catalysis.[57−60] Furthermore, it was widely believed that the Ca promoter increased the numbers of the basic sites on the surface of the catalysts and then strengthened the chemisorption of the CO_2, which had been confirmed by the CO_2-TPD analysis (refer to Figure 6).

As the dosage of the Ca was lowered, the chemisorption and activation of the CO_2 were simultaneously promoted. However, an excessive addition of Ca inhibited the catalytic activities. Similar situations were also encountered in the pioneer literature with K_2O, Cs_2O, CaO, MgO, BaO, La_2O_3, and so on, as promoters.[37,39−41,61] When the number of the basic sites was superfluous, the chemisorbed CO_2 would cover the Ni active sites of the catalysts, and the chemical adsorption from the active sites became difficult due to the strong alkaline sites among the frameworks of the catalysts. Consequently, the subsequent adsorption and activation of the CO_2 were blocked, finally leading to a decline in the CH_4 and CO_2 conversions. Meanwhile, the previous work also pointed out that a higher concentration of the basic centers would cover a certain amount of the Ni active sites; block the accessibility of the methane; and finally, result in a decrease in the reforming activity.[39] In summary, the catalytic behavior of the catalyst was the result of the synergy effect of the size, structure, composition, and so on.[12] Therefore, the improved catalytic activity could be obtained only when the dosage of the basic promoter (CaO) was moderate.

3.2.3. Long-Term Stability Test of the Catalyst. Recently, developing stable catalysts has been the essential issue in the CRM reaction. The evaluation of the long-term stabilities of the catalysts was performed under given conditions: CH_4/CO = 1, 700 °C, GHSV = 15 000 mL/(g·h), 1 atm. M-5Ni95Al and M-5Ni5Ca90Al were selected as the representatives for the catalysts without and with basic modifications, respectively. As shown in Figure 9(1), (2), both M-5Ni95Al and M-5Ni5Ca95Al catalysts exhibited high catalytic activities (e.g., around 78%, 81% for the conversions of CH_4, CO_2 over M-5NiCa95Al, respectively) and stable catalytic behavior in the whole 50 h time on stream. As mentioned above, the excellent catalytic activities of the mesoporous catalysts should be attributed to the merits of the mesostructures, which would accommodate the gaseous reactants with many more "exposed" or "accessible" Ni active centers than traditional supported catalysts. As for the CRM reaction itself, its fatal drawback was that the reforming catalysts were mainly subjected to several deactivation mechanisms, including coking, sintering, and oxidation of the metallic phase, which would result in a decrease in the active metal sites on the catalyst surface and ultimately lower the catalytic stability. But it was also believed that the Ni particles with smaller size possessed strengthened capability to suppress the carbon deposition.[2,3,12,24]

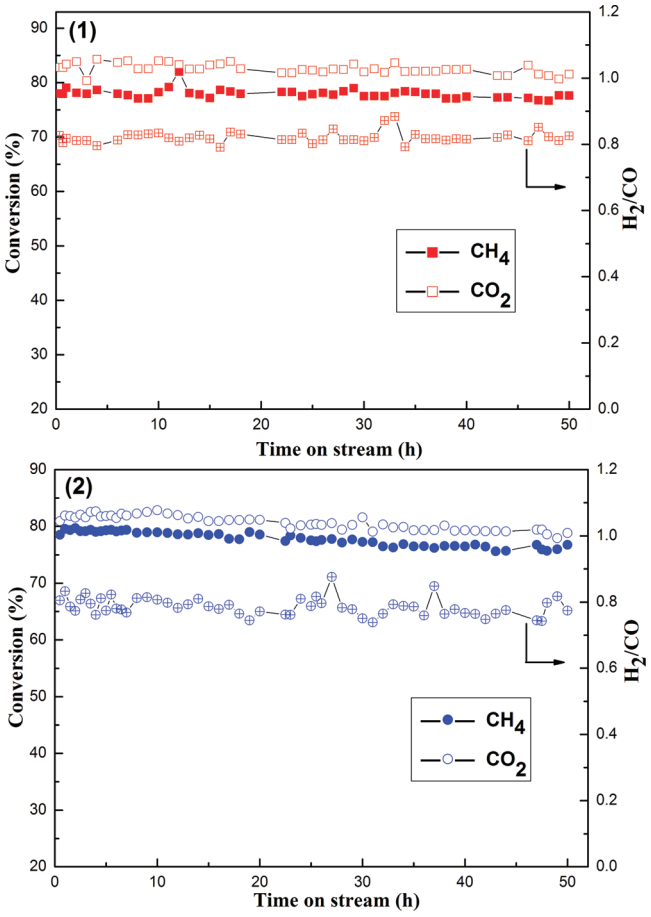

Figure 9. Long-term stability tests over the M-5Ni95Al and M-5Ni5Ca90Al catalysts; Reaction conditions: CH_4/CO_2 = 1, GHSV = 15 000 mL/(g·h), 700 °C, 1 atm.

As for the above-mentioned mesoporous catalysts, the Ni active sites were embedded in the mesoporous skeletons due to the advantage of the one-pot strategy. Therefore, the "confinement effect" of the mesopores played very important roles in limiting the growth of the Ni nanoparticles during the processes of reduction and reaction.[62,63] As a result, the catalytic stabilities of the mesoporous catalysts were promoted due to the "size effect" of the Ni nanoparticles. In addition to this, the modified Ca improved the Lewis basicity and favored the chemisorption of CO_2 over the M-5Ni5Ca90Al catalyst, which would further accelerate the procedure $CO_2 + C = 2CO$

dx.doi.org/10.1021/cs3001072 | ACS Catal. 2012, 2, 1331−1342

and then reduce the carbon deposition. Consequently, the excellent catalytic activities of M-5Ni95Al and M-5Ni5Ca90Al for long-term stabilities were preserved as a result of their high coke resistance abilities.

3.3. Characterization of the As-Reduced, The Used, And Endurance-Tested M-5Ni*x*Ca(95 − *x*)Al Catalysts. *3.3.1. Comparative Analyses of the WXRD Patterns for the As-Reduced, The Used, And the Endurance-Tested M-5Ni5Ca90Al.* The comparative analyses of the WXRD for the as-reduced, the used, and the endurance-tested M-5Ni5Ca90Al were conducted, and their patterns are displayed in Figure 10.

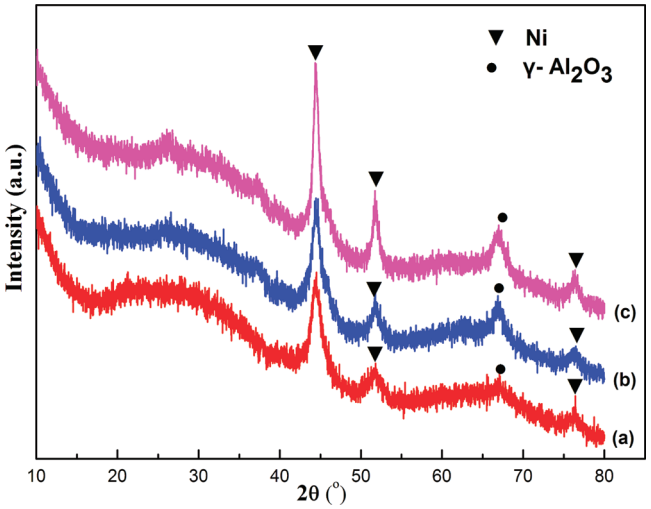

Figure 10. Wide-angle X-ray diffraction patterns for the M-5Ni5Ca90Al catalyst after different treatments: (a) the as-reduced catalyst, (b) the used catalyst, (c) the endurance-tested catalyst.

Typically, the as-reduced catalyst was the catalyst reduced at 800 °C in a mixed flow of H_2/N_2 (10:20 mL/min) for 2 h and cooled to room temperature in a nitrogen atmosphere. The used catalyst was the catalyst tested under these conditions: CH_4/CO_2 = 1, GHSV=15 000 mL/(g·h), 1 atm, and temperatures from 600 to 800 °C at increments of 50 °C and remaining at each temperature stage for 70 min. The endurance-tested catalyst was the catalyst that experienced a 50 h lifetime stability test under these given conditions: CH_4/CO_2 = 1, 700 °C, GHSV = 15000 mL/(g·h), 1 atm.

Compared with the as-synthesized M-5Ni5Ca90Al (see Figure 1(2)), the phase transition from amorphous to γ phase for the alumina mesoporous skeleton took place for the as-reduced sample due to the appearance of diffraction peaks of γ-Al_2O_3 (JCPDS Card No. 10-0425) after being reduced at 800 °C for 2 h. In addition, the characteristic diffraction peaks of the Ni (JCPDS Card No. 87-0712) were detected in the as-reduced M-5Ni5Ca90Al. However, it was difficult to calculate its crystallite size because of the broadening of the diffraction peaks, illuminating the high dispersion of the Ni nanoparticles.

Compared with the as-reduced M-5Ni5Ca90Al, the used M-5Ni5Ca90Al presented only a bit stronger γ-Al_2O_3 diffraction intensity after under undergoing different temperature stages. Nevertheless, the diffraction intensities of the metallic Ni in these two patterns were greatly similar, suggesting that the thermal sintering of the Ni nanoparticles was avoided to some degree.

Compared with the aforementioned two samples, the grain size of the Ni nanoparticles of the endurance-tested M-5Ni5Ca90Al showed a remarkable increase, whereas the average $D_{(200)}$ (D is the crystallite size) of the Ni particles was only 8.15 nm and still preserved its nanosized state. The "confinement effect" of the mesoporous framework contributed the stabilization of the metallic nanoparticles. In addition to this, no graphic carbon diffraction peak was observed in the patterns of the used as well as endurance-tested samples, which was evidence of the high anticoke capacity of the catalyst.

3.3.2. Comparative Analysis of the Textural Properties for the As-Reduced, The Used, And the Endurance-Tested M-5Ni5Ca90Al. To investigate the thermal stability of the M-5Ni*x*Ca(95 − *x*)Al materials, the textural properties of the as-reduced, the used, and the endurance-tested samples were also carefully characterized. The M-5Ni5Ca90Al was also selected as an example, and the characterization results of the nitrogen adsorption−desorption analysis are presented in Figure 11. As

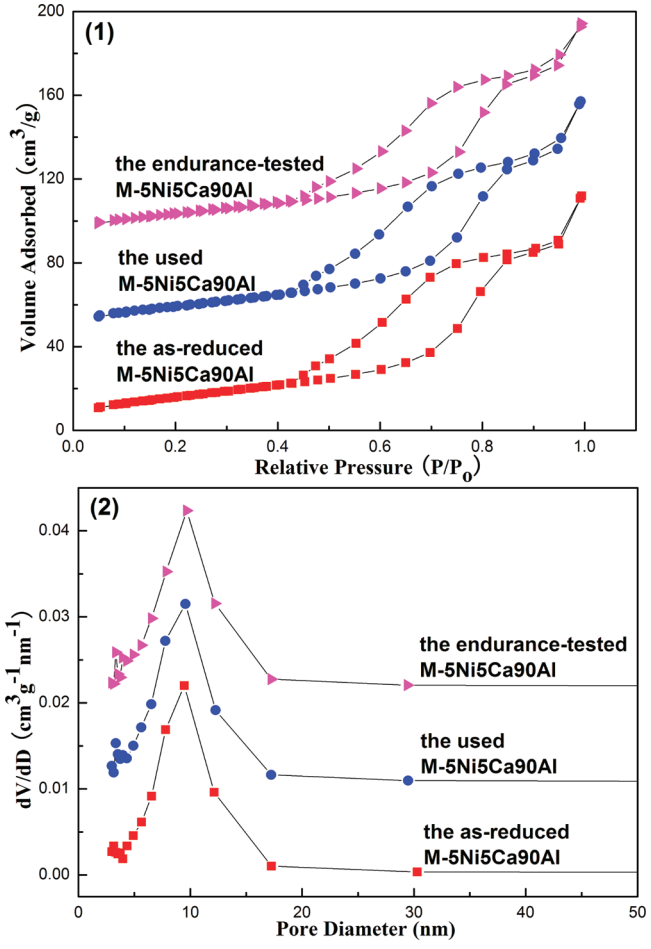

Figure 11. Isotherms (1) and pore size distributions (2) of the M-5Ni5Ca90Al catalyst after different treatments.

shown in the figure, the as-reduced, the used, and even the 50 h endurance-tested samples all displayed type IV isotherms, with an H1-shaped hysteresis loop, which indicates that the uniform cylindrical mesopore channels were still preserved after various treatments. Furthermore, their pore size distributions were also extremely narrow: around 9.50 nm. Hence, the ordered mesoporous structure of the M-5Ni5Ca90Al was successfully maintained after high temperature reduction and severe reaction processes.

dx.doi.org/10.1021/cs3001072 | ACS Catal. 2012, 2, 1331−1342

Moreover, the structural properties of these materials are also summarized in Table 1. Compared with the as-synthesized M-5Ni5Ca90Al, the specific surface areas and pore volumes showed some decrease due to the phase transformation of the alumina substrate from amorphous to γ phase under harsh reduction conditions, according to the XRD analysis (refer to Figure 10), whereas, compared with the as-reduced M-5Ni5Ca90Al, the used and the 50 h endurance-tested samples took on similar specific surface areas and pore volumes, suggesting that the carbon deposition over these samples was so negligible that it did not block the mesopores. In addition, the average pore diameters of the as-reduced, the used, and the 50 h endurance-tested M-5Ni5Ca90Al were all similar to that of the as-synthesized sample, illustrating that the shrinkage of the skeleton of the material was avoided to some degree. Although the specific surface areas and pore volumes suffered from a certain decrease during the harsh reduction and reaction conditions, yet their uniform mesostructures and pore size distributions were successfully preserved. Therefore, evidence mentioned above once again demonstrated the predominant thermal stability of this series of materials.

3.3.3. TG–DSC Analysis of the 50 h Endurance-Tested M-5Ni95Al and M-5Ni5Ca90Al Catalysts. The properties of the carbon deposition over M-5Ni95Al and M-5Ni5Ca90Al catalysts after 50 h long-term stability tests at 700 °C are shown in Figure 12. As for the TG curves in Figure 12 (1), with the increase in the temperature, the general trend of the curves was downward; however, the curve of the M-5Ni5Ca90Al experienced a slight rise in the region from 200 to 600 °C, which might be derived from the oxidation of the metallic Ni.[40,48] The TG curve of the spent catalyst indicated the weight loss due to the removal of the deposited carbon. The TG curves showed that the weight loss of the coke over M-5Ni95Al was much higher than that of the M-5Ni5Ca90Al, implying that the modification of the Ca element indeed contributed to the suppression and elimination of the coke during the CRM reaction. As for the mechanism of the carbon deposition over CRM reaction, it was commonly believed that metallic Ni^0 possessed an unfilled d orbital, which can accept a C–H σ electron of the CH_4 molecule during the adsorption of CH_4, then weaken or even break the C–H bond of the CH_4 and, finally, lead to carbon deposition on the surface of the metallic Ni^0. The modified Ca ought to play dual roles in preventing the carbon deposition for the CRM reaction. One one hand, the Ca could greatly decrease the acidity of the catalyst; therefore, the formation of the pyrolytic carbon depending on the surface acidity was effectively prevented. On the other hand, the basic Ca favored the chemisorbed activation and dissociation of CO_2 and subsequently accelerated the carbon elimination via the reaction $CO_2 + C = 2CO$.

The DSC profiles in Figure 12(2) exhibited that the deposition carbon could be completely burned up in a temperature range between 200 and 800 °C. One weak shoulder exothermic peak around 300–340 °C and another pronounced exothermic peak around 610–670 °C could be observed for all the samples, implying that at least two sorts of the coke deposited on the surface of the catalysts. The weak exothermic peaks in the range of 300–340 °C might derive from the combustion of the amorphous carbon, which contributed to the formation of the synthesis gas.[64,65] Another group of the exothermic peaks around 610–670 °C could be ascribed to the combustion of the carbon nanotube (also known as filament carbon), which was responsible for the

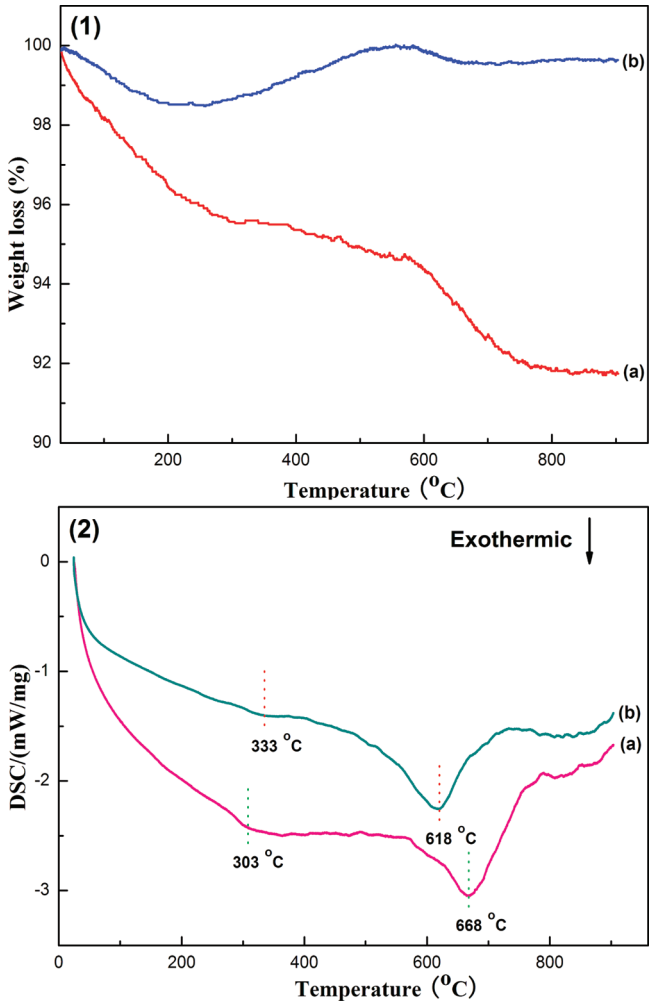

Figure 12. TG (1) and DSC (2) curves of the 50 h endurance-tested catalysts: (a) M-5Ni95Al, (b) M-5Ni5Ca90Al.

deactivation of the catalyst, according to the pioneer literature.[66] In addition, it was of great interest to find that the intensity of the M-5Ni5Ca90Al's DSC curve was much weaker than that of the M-5Ni95Al's. As well-known, the exothermic peaks were mainly derived from the combustion of the coke deposited on the catalyst. Thus, this phenomenon once again illuminated that the amount of the carbon deposition over the M-5Ni5Ca90Al was greatly lower than that over the M-5Ni95Al from another aspect. Generally, the curves of the DSC were in good agreement with those of the TG.

3.3.4. Morphology Analysis of the 50 h Endurance-Tested M-5Ni5Ca90Al Catalyst. To further confirm the morphology of the coke as well as the outstanding thermal stability of the present material, TEM analysis of the 50 h endurance-tested M-5Ni5Ca90Al was performed. The images are displayed in Figure 13. The uniform cylindrical mesopores along the [110] and [001] directions were clearly observed from Figure 13(a) and (b), respectively, indicating that the ordered mesostructure of the M-5Ni5Ca90Al was successfully maintained. The ordered mesopores also confirmed the deduction based on the IV H1-shaped hysteresis loops in the previous section.

As shown in Figure 13c, the coke residue over the spent catalyst observed was the carbon nanotubes. Moreover, it is worth noting that no carbon nanotubes were observed among

dx.doi.org/10.1021/cs3001072 | ACS Catal. 2012, 2, 1331–1342

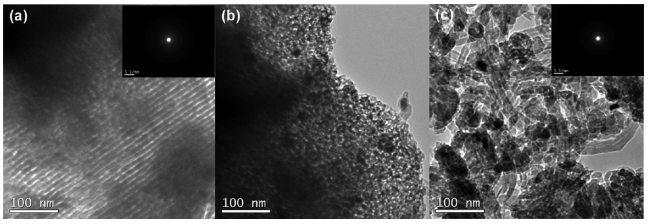

Figure 13. TEM pictures of the 50 h endurance-tested M-5Ni5Ca90Al catalyst.

the mesopores, according to Figure 13a and b, which denotes that the carbon nanotubes were mainly distributed outside the mesopores. Consequently, the deactivation of the catalyst deriving from the coverage of Ni active centers by the coke was effectively avoided to some degree, accounting for no deactivation after the 50 h lifetime endurance test. It is also of interest that no obvious amorphous carbon was observed. The reason for this might be that the amorphous carbon was evenly distributed among the mesopores and could be in situ eliminated in the subsequent process of CO production. The TEM images (parts a, b) once again demonstrated the prominent thermal stability of the current ordered mesoporous materials. The presence of the carbon nanotubes further confirmed the deduction based on the TG−DSC analyses.

4. CONCLUSION

Ordered mesoporous tricompound NiO−CaO−Al_2O_3 composite oxides with different Ca contents were originally designed and facilely prepared via a one-pot evaporation-induced self-assembly strategy. The obtained materials possessing excellent textural properties and thermal stabilities were utilized as the catalysts for CRM reaction. These mesoporous catalysts entirely exhibited excellent catalytic activities and long catalytic stabilities. The ordered mesoporous framework played a significant role in endowing these merits for these catalysts, which could provide more "accessible" Ni active centers for the gaseous reactants and stabilize the Ni nanoparticles by the "confinement effect" under severe reduction and reaction conditions. The modification of Ca among the mesoporous skeletons also acted as a key factor in improving the catalytic performances as well as suppressing carbon deposition by enhancing the chemisorbed activation of the CO_2. Because of these advantages, these ordered mesoporous NiO−CaO−Al_2O_3 composite oxides promise a series of ideal catalyst candidates for the CRM reaction.

AUTHOR INFORMATION

Corresponding Author

*Phone: +86 931 4968066. Fax: +86 931 4968129. E-mail: ljchou@licp.cas.cn.

Notes

The authors declare no competing financial interest.

ACKNOWLEDGMENTS

The authors sincerely acknowledge financial support from the National Basic Research Program of P. R. China (No. 2011CB201404) and the National Natural Science Foundation of China (No. 21133011).

REFERENCES

(1) Ashcroft, A. T.; Cheetham, A. K.; Green, M. L. H.; Vernon, P. D. F. *Nature* **1991**, *352*, 225.
(2) Bradford, M. C. J.; Vannice, M. A. *Cat. Rev.−Sci. Eng.* **1999**, *41*, 1.
(3) Hu, Y. H.; Ruckenstein, E. *Cat. Rev.−Sci. Eng.* **2002**, *44*, 423.
(4) Song, C. S. *Catal. Today* **2006**, *115*, 2.
(5) Zhang, J.; Wang, H.; Dalai, A. K. *J. Catal.* **2007**, *249*, 300.
(6) Fan, M. S.; Abdullah, A. Z.; Bhatia, S. *Appl. Catal., B* **2010**, *100*, 365.
(7) Prieto, G.; Concepcion, P.; Martinez, A.; Mendoza, E. *J. Catal.* **2011**, *280*, 274.
(8) Ross, J. R. H.; van Keulen, A. N. J.; Hegarty, M. E. S.; Seshan, K. *Catal. Today* **1996**, *30*, 193.
(9) Xu, B. Q.; Sachtler, W. M. H. *J. Catal.* **1998**, *180*, 194.
(10) Levy, M.; Levitan, R.; Meirovitch, E.; Segal, A.; Rosin, H.; Rubin, R. *Sol. Energy* **1992**, *48*, 395.
(11) Levy, M.; Rubin, R.; Rosin, H.; Levitan, R. *Energy* **1992**, *17*, 749.
(12) Liu, C. J.; Ye, J.; Jiang, J.; Pan, Y. *ChemCatChem* **2011**, *3*, 529.
(13) Hu, Y. H.; Ruckenstein, E. *Adv. Catal.* **2004**, *48*, 297.
(14) Rostrupnielsen, J. R.; Hansen, J. H. B. *J. Catal.* **1993**, *144*, 38.
(15) Bradford, M. C. J.; Vannice, M. A. *J. Catal.* **1999**, *183*, 69.
(16) Sigl, M.; Bradford, M. C. J.; Knozinger, H.; Vannice, M. A. *Top. Catal.* **1999**, *8*, 211.
(17) Nakamura, J.; Aikawa, K.; Sato, K.; Uchijima, T. *Catal. Lett.* **1994**, *25*, 265.
(18) Damyanova, S.; Pawelec, B.; Arishtirova, K.; Martinez Huerta, M. V.; Fierro, J. L. G. *Appl. Catal., B* **2009**, *89*, 149.
(19) Zhang, Z. L.; Tsipouriari, V. A.; Efstathiou, A. M.; Verykios, X. E. *J. Catal.* **1996**, *158*, 51.
(20) Solymosi, F.; Kutsan, G.; Erdohelyi, A. *Catal. Lett.* **1991**, *11*, 149.
(21) Tomishige, K.; Yamazaki, O.; Chen, Y. G.; Yokoyama, K.; Li, X. H.; Fujimoto, K. *Catal. Today* **1998**, *45*, 35.
(22) Wei, J. M.; Xu, B. Q.; Li, J. L.; Cheng, Z. X.; Zhu, Q. M. *Appl. Catal., A* **2000**, *196*, L167.
(23) Gadalla, A. M.; Bower, B. *Chem. Eng. Sci.* **1988**, *43*, 3049.
(24) Hu, Y. H. *Catal. Today* **2009**, *148*, 206.
(25) Roh, H. S.; Jun, K. W. *Catal. Surv. Asia* **2008**, *12*, 239.
(26) Zhu, X.; Huo, P.; Zhang, Y. P.; Cheng, D. G.; Liu, C. J. *Appl. Catal., B* **2008**, *81*, 132.
(27) Xu, B. Q.; Wei, J. M.; Yu, Y. T.; Li, Y.; Li, J. L.; Zhu, Q. M. *J. Phys. Chem. B* **2003**, *107*, 5203.
(28) Carreon, M. A.; Guliants, V. V. *Eur. J. Inorg. Chem.* **2005**, 27.
(29) van Dillen, A. J.; Terorde, R.; Lensveld, D. J.; Geus, J. W.; de Jong, K. P. *J. Catal.* **2003**, *216*, 257.
(30) Liu, B. S.; Au, C. T. *Appl. Catal., A* **2003**, *244*, 181.
(31) Sierra Gallego, G.; Mondragon, F.; Barrault, J.; Tatibouet, J. M.; Batiot-Dupeyrat, C. *Appl. Catal., A* **2006**, *311*, 164.
(32) Xu, Z. L.; Zhen, M.; Bi, Y. L.; Zhen, K. J. *Appl. Catal., A* **2000**, *198*, 267.
(33) Xu, Z. L.; Zhen, M.; Bi, Y. L.; Zhen, K. J. *Catal. Lett.* **2000**, *64*, 157.
(34) Luna, A. E. C.; Iriarte, M. E. *Appl. Catal., A* **2008**, *343*, 10.
(35) Hu, Y. H.; Ruckenstein, E. *Catal. Lett.* **1997**, *43*, 71.
(36) Yamazaki, O.; Nozaki, T.; Omata, K.; Fujimoto, K. *Chem. Lett.* **1992**, 1953.
(37) Liu, S.; Guan, L.; Li, J.; Zhao, N.; Wei, W.; Sun, Y. *Fuel* **2008**, *87*, 2477.
(38) Hou, Z. Y.; Yashima, T. *Appl. Catal., A* **2004**, *261*, 205.
(39) Chen, P.; Hou, Z. Y.; Zheng, X. M. *Chin. J. Chem.* **2005**, *23*, 847.
(40) Xu, L.; Song, H.; Chou, L. *Appl. Catal., B* **2011**, *108*, 177.
(41) Yang, R.; Xing, C.; Lv, C.; Shi, L.; Tsubaki, N. *Appl. Catal., A* **2010**, *385*, 92.
(42) Zhang, W. D.; Liu, B. S.; Zhan, Y. P.; Tian, Y. L. *Ind. Eng. Chem. Res.* **2009**, *48*, 7498.
(43) Yuan, Q.; Yin, A. X.; Luo, C.; Sun, L. D.; Zhang, Y. W.; Duan, W. T.; Liu, H. C.; Yan, C. H. *J. Am. Chem. Soc.* **2008**, *130*, 3465.
(44) Morris, S. M.; Fulvio, P. F.; Jaroniec, M. *J. Am. Chem. Soc.* **2008**, *130*, 15210.

(45) Beck, J. S.; Vartuli, J. C.; Roth, W. J.; Leonowicz, M. E.; Kresge, C. T.; Schmitt, K. D.; Chu, C. T. W.; Olson, D. H.; Sheppard, E. W.; McCullen, S. B.; Higgins, J. B.; Schlenker, J. L. *J. Am. Chem. Soc.* **1992**, *114*, 10834.
(46) Kresge, C. T.; Leonowicz, M. E.; Roth, W. J.; Vartuli, J. C.; Beck, J. S. *Nature* **1992**, *359*, 710.
(47) Cai, W.; Yu, J.; Anand, C.; Vinu, A.; Jaroniec, M. *Chem. Mater.* **2011**, *23*, 1147.
(48) Xu, L.; Song, H.; Chou, L. *Catal. Sci. Technol.* **2011**, *1*, 1032.
(49) Oh, Y. S.; Roh, H. S.; Jun, K. W.; Baek, Y. S. *Int. J. Hydrogen Energy* **2003**, *28*, 1387.
(50) Chu, Y. L.; Li, S. B.; Lin, J. Z.; Gu, J. F.; Yang, Y. L. *Appl. Catal., A* **1996**, *134*, 67.
(51) Zhang, K.; Zhou, G.; Li, J.; Zhen, K.; Cheng, T. *Catal. Lett.* **2009**, *130*, 246.
(52) Zhang, S.; Wang, J.; Liu, H.; Wang, X. *Catal. Commun.* **2008**, *9*, 995.
(53) Tomiyama, S.; Takahashi, R.; Sato, S.; Sodsawa, T.; Yoshida, S. *Appl. Catal., A* **2003**, *241*, 349.
(54) Mile, B.; Stirling, D.; Zammitt, M. A.; Lovell, A.; Webb, M. *J. Catal.* **1988**, *114*, 217.
(55) Dias, J. A. C.; Assaf, J. M. *Catal. Today* **2003**, *85*, 59.
(56) Pino, L.; Vita, A.; Cipiti, F.; Lagana, M.; Recupero, V. *Appl. Catal., B* **2011**, *104*, 64.
(57) Arico, A. S.; Antonucci, P. L.; Modica, E.; Baglio, V.; Kim, H.; Antonucci, V. *Electrochim. Acta* **2002**, *47*, 3723.
(58) Weber, A. P.; Seipenbusch, M.; Kasper, G. *J. Nanopart. Res.* **2003**, *5*, 293.
(59) Bang, Y.; Seo, J. G.; Song, I. K. *Int. J. Hydrogen Energy* **2011**, *36*, 8307.
(60) Lee, J.; Hwang, S.; Seo, J. G.; Hong, U. G.; Jung, J. C.; Song, I. K. *J. Ind. Eng.Chem.* **2011**, *17*, 310.
(61) Rezaei, M.; Alavi, S. M.; Sahebdelfar, S.; Yan, Z. F. *Energy Fuels* **2008**, *22*, 2195.
(62) Sun, N.; Wen, X.; Wang, F.; Wei, W.; Sun, Y. *Energy Environ. Sci.* **2010**, *3*, 366.
(63) Zhang, M.; Ji, S.; Hu, L.; Yin, F.; Li, C.; Liu, H. *Chin. J. Catal.* **2006**, *27*, 777.
(64) Chen, Y. G.; Ren, J. *Catal. Lett.* **1994**, *29*, 39.
(65) Swaan, H. M.; Kroll, V. C. H.; Martin, G. A.; Mirodatos, C. *Catal. Today* **1994**, *21*, 571.
(66) Wang, S. B.; Lu, G. Q. *Energy Fuels* **1998**, *12*, 248.